Electronic Supplementary Information

Significant Improvement in High-Temperature Energy Storage Performance of Polymer Dielectrics *via* Constructing Surface Polymer Carrier Trap Layer

Jie Xiong[a], Xing Fan[a], Dajiang Long[a], Bofeng Zhu[b], Xiao Zhang[b]*, Junyong Lu[b], Yunchuan Xie[a] and Zhicheng Zhang[a]*

[a] Xi'an Key Laboratory of Sustainable Energy Materials Chemistry, School of chemistry; Xi'an Jiaotong University; Xi'an, P. R. China, 710049.

[b] National Key Laboratory of Science and Technology on Vessel Integrated Power System; Naval University of Engineering; Wuhan, P. R. China, 430033.

Experimental section

Materials

The 5.5 μm BOPP purchased from Quan Zhou Jia De Li Electronies Material Co. Ltd. as deposition substrate in this paper. The Parylene N, C and F dimers were purchased from Su Zhou Pai Hua Layer Co., Ltd. All the other chemicals are commercially available and used as received until notified specially.

Preparation of Surface Functionalized Films

Typical CVD surface deposition includes the following three steps:

(1) Vaporizer: The process starts with granular dimer. The parylene dimer is vaporized from a solid directly into a parylene dimeric gas. Temperature is 150-200°C.

(2) Pyrolysis: The dimeric gas is heated to split the dimer molecule and produce a monomeric gas. Temperature is 600-700°C.

(3) Polymerisation: Finally, the monomer gas is released into the coating chamber and deposited on the substrate surface to form a transparent polymer film. Deposition temperature is at room temperature, pressure is 30-50 mTorr, and deposition rate is 0.5-5 μm/h.

The BOPP-XS film requires a CVD polymer process on only one side of the BOPP film, whereas the BOPP-X film requires a CVD polymerization process on both sides of the BOPP film. Controlling of parylene thickness is achieved by adjusting deposition time.

Instruments and characterization

Fourier transform infrared (FTIR) spectroscopy of the film was recorded on a Tensor 27 (Bruker, Germany) using the Attenuated Total Reflection (ATR) mode in the range of 4000 cm^{-1}–400 cm^{-1} to identify the chemical composition of samples. X–ray photoelectron spectroscopy (XPS) was recorded using X–ray photoelectron spectra (Thermo Fisher ESCALAB Xi^{+}) with an Al Kα source. Field–emission scanning electron microscopy (FE–SEM) results were obtained on ZEISS GeminiSEM 500, and the samples were coated with a thin layer of gold before observation. Energy Dispersive X–ray Spectroscopy (EDS) mapping of a selected area in an SEM image was performed on the same instrument as SEM. Element

mapping images and EDS spectra of mapped areas were recorded. For electric properties characterizations, gold electrodes with a thickness of 50–80 nm were sputtered on both surfaces of the polymer films with a JEOL JFC–1600 auto fine coater (Japan). The surface morphology of films was obtained by atomic force microscopy (AFM) (Dimension Icon, Bruker, Germany) in tapping mode. Broadband dielectric spectroscopy (BDS) was performed on a Novocontrol Concept 80 broadband dielectric spectrometer with temperature control. Storage modulus (E') and loss factor (tanδ) were obtained by dynamic mechanical analysis (DMA). For the investigations, a dynamic mechanical analyzer Netzsch DMA242E (Netzsch, Germany) was utilized. Measurements were performed in tensile mode at a constant frequency of 1 Hz. The temperature was varied between 30 and 180°C at a constant rate of 4°C min^{-1}. Prismatic samples of about 5 mm in width and 10 mm in length were used. The applied voltage was 1 V with the frequency changing from 10^0 Hz to 10^6 Hz and the temperature was increased from 20°C to 150°C at a rate of 4 °C min^{-1}; the electrode diameter of the test sample is 1 cm. The electric D–E hysteresis loops were collected on a Premiere II ferroelectric tester from Radiant Technologies, Inc. at room temperature, where AC electric fields ranging from 50 to 800 MV m^{-1} were applied across the polymer films with a triangular waveform at a frequency of 10 Hz. The breakdown electric field for polymer films was determined by the breakdown voltage tester (Beijing Beiguangjingyi Instrument Equipment Co. Ltd.) and the electric field applied rate of 1 kV min^{-1}. The diameter of the cylindrical electrode was 10 mm. The leakage current was obtained as less than 10 mA until the polymer films were broken down. Charge–discharge tests were performed using a PKCPR1502 test system (PolyK Technologies) with an applied electric field of 300 MV m^{-1} and resistance of load resistor of 100 kΩ. The charge–discharge cycle was controlled by a LabVIEW program.

The film samples were charged by isothermal surface potential decay (ISPD), and the needle tip was separated from the grid. The electrode is 5 mm, and the grid is 5 mm from the surface of the sample. The potentiometer was a Trek P0865 made in the United States, about 3 mm from the surface of the sample, and was placed in an

incubator with the entire electrode system. The charging voltages applied to the needle electrode and the grid were –12 kV and –2 kV, respectively, charging for 10 min, then removing the voltage source, and moving the sample under the electrostatic probe for measurement. The test time was 2 h.

The ISPD method was used to study the distribution of trapped carriers. The important relationship between the energy level (E_T) and trapped charge density [$Q_s(t)$] could be derived and calculated [S1-3]:

$$E_T = k_B T ln(v_{ATE} t) \quad \text{(S1)}$$

$$Q_s(t) = t\frac{\varepsilon_0 \varepsilon_r d\emptyset_s(t)}{q_e L \quad dt} \quad \text{(S2)}$$

Where k_B is Boltzmann's constant, T is the temperature where the material is placed, v_{ATE} is the attempt–to–escape frequency, t represents the decay time of the surface potential, ε_0 is the vacuum dielectric constant, ε_r is the relative dielectric constant, $\phi_s(t)$ is the time–dependent surface potential of the material, L is the thickness of the thin film sample. As we can see from **equation (S1)**, the energy level is associated with Boltzmann's constant, Kelvin temperature, attempt–to–escape frequency and decay time. As shown in **equation (S2)**, the trapped charge density is related to the permittivity and thickness of the sample, the decay rate of the ISPD curve and the decay time.

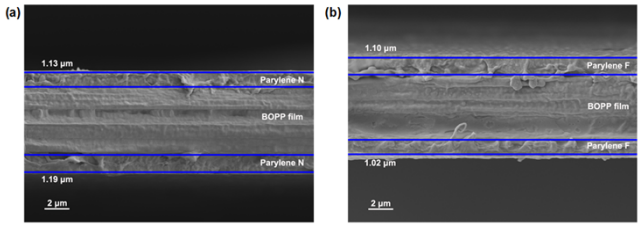

Fig. S1. Cross-sectional SEM images of (a) BOPP-N and (b) BOPP-F film.

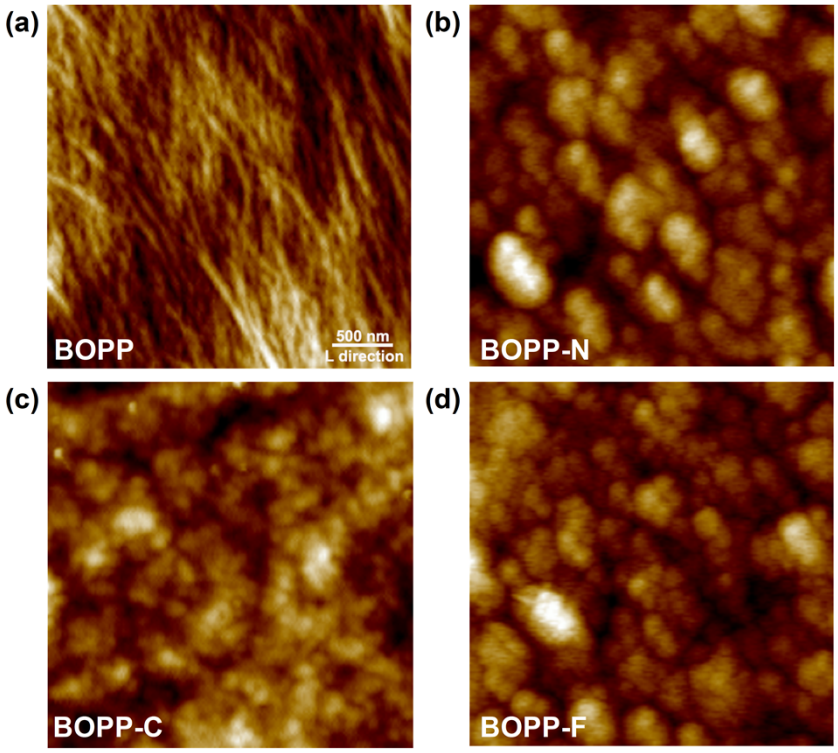

Fig. S2. The AFM topographic images of the pristine BOPP and BOPP–X films (scanning area: 3.0 × 3.0 μm^2).

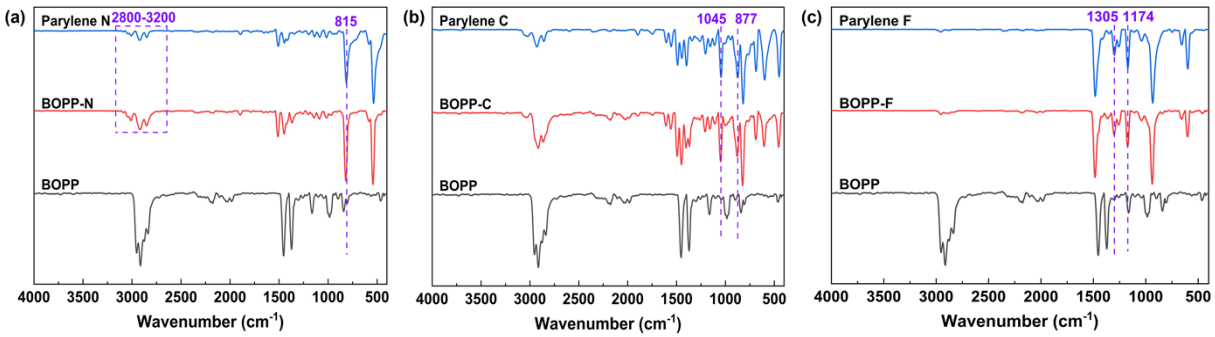

Fig. S3. FTIR spectra of the pristine BOPP, parylene polymer films and the surface-functionalized BOPP films.

Table S1. The main chemical bonds assignment of the surface-functionalized BOPP films

Sample	Wavenumber(cm^{-1})	Assignment
BOPP–N	2800–3200	C–H bond in aromatic ring vibrations
	815	Two neighboring H atoms bonded to aromatic ring vibrations
BOPP–C	1045	Cl bonded to aromatic ring vibrations
	877	Cl bonded to aromatic ring vibrations
BOPP–F	1305	C–F stretching on the benzene ring
	1174	C–F stretching on the benzene ring

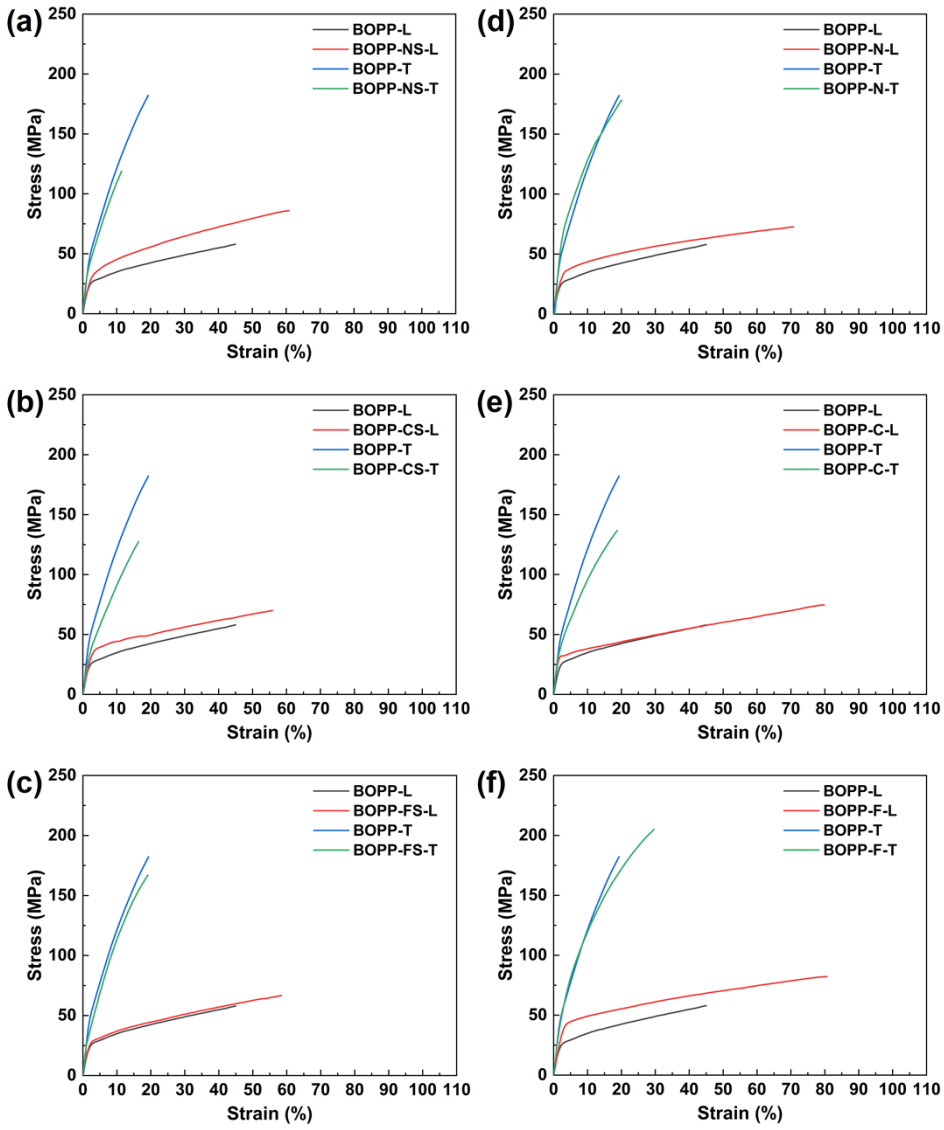

Fig. S4. The stress–strain curves of the pristine BOPP and the surface-functionalized BOPP films.

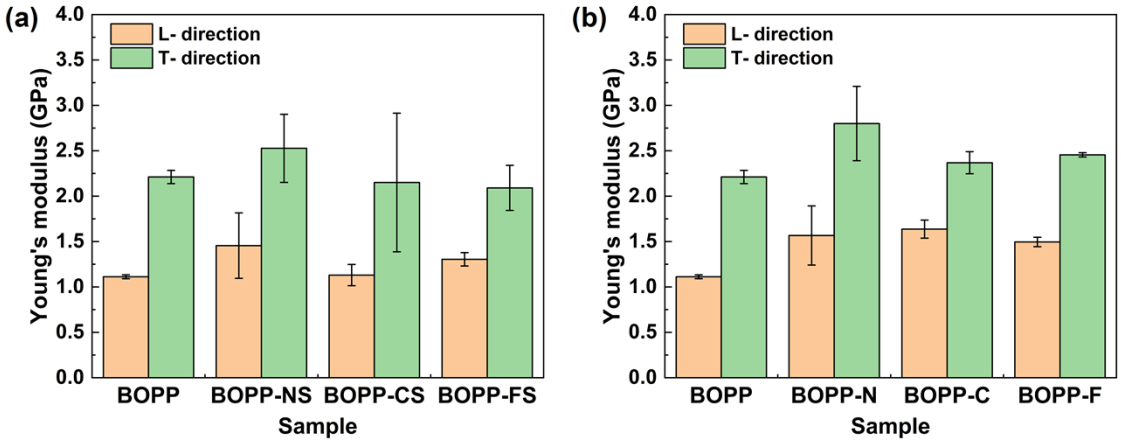

Fig. S5. The Young's modulus of BOPP, BOPP–XS and BOPP–X films.

Table S2. The mechanical properties of the pristine BOPP and the surface-functionalized BOPP films.

Sample	Breaking elongation/%	Tensile strength/MPa
BOPP	44.98 (L, ±11.89)	57.97 (L, ±3.94)
	19.31 (T, ±4.50)	182.13 (T, ±18.71)
BOPP–NS	60.82 (L, ±1.27)	86.04 (L, ±21.23)
	11.44 (T, ±2.31)	118.93 (T, ±19.04)
BOPP–CS	55.85(L, ±5.43)	69.89 (L, ±28.423)
	16.43 (T, ±3.30)	127.40 (T, ±13.20)
BOPP–FS	58.42(L, ±2.81)	66.68 (L, ±1.98)
	19.09 (T, ±1.07)	166.87 (T, ±11.673)
BOPP–N	70.74 (L, ±8.13)	72.69 (L, ±8.96)
	20.09 (T, ±2.17)	178.20 (T, ±12.70)
BOPP–C	79.78 (L, ±6.32)	74.25 (L, ±9.36)
	18.77 (T, ±4.22)	136.77 (T, ±22.77)
BOPP–F	80.58 (L, ±1.58)	82.18 (L, ±8.58)
	29.57 (T, ±1.75)	204.95 (T, ±19.11)

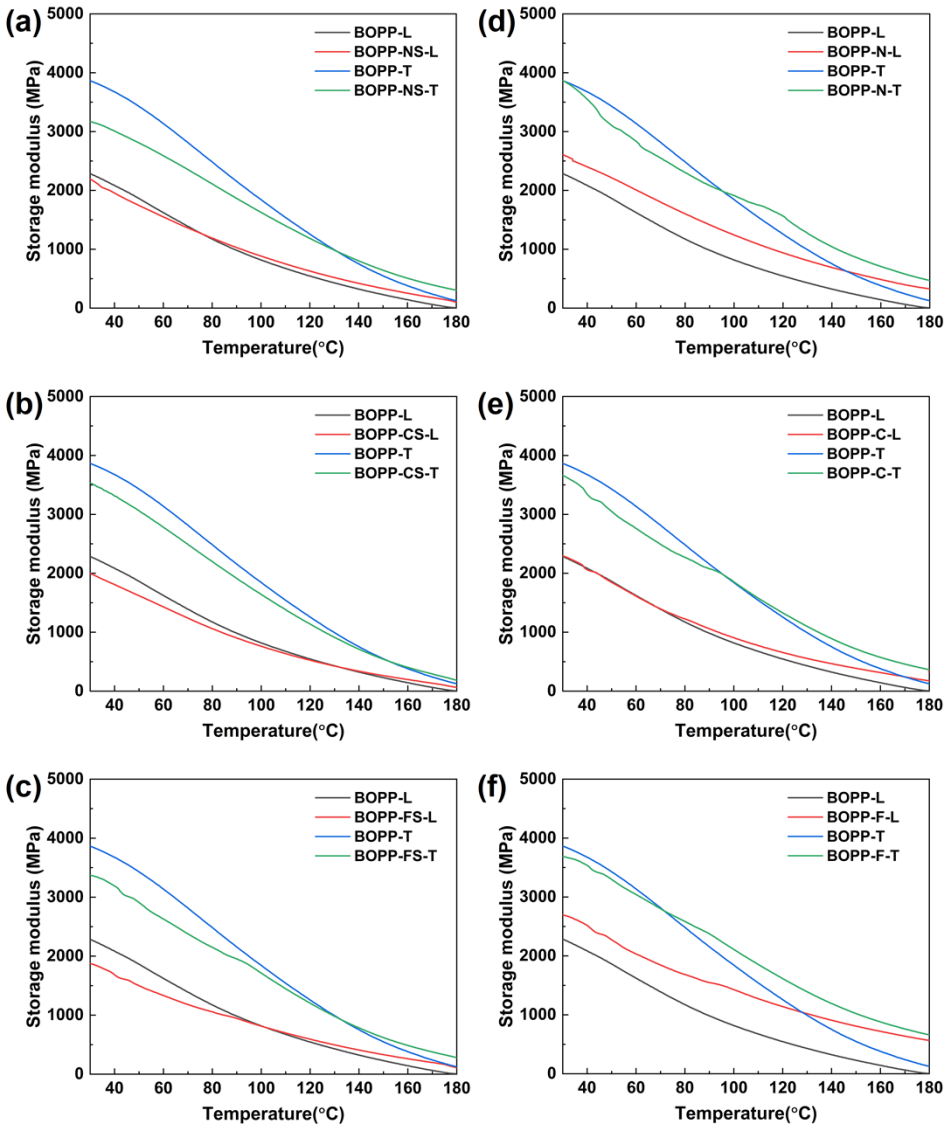

Fig. S6. Temperature dependence of storage modulus of the pristine BOPP, BOPP–XS and BOPP–X films.

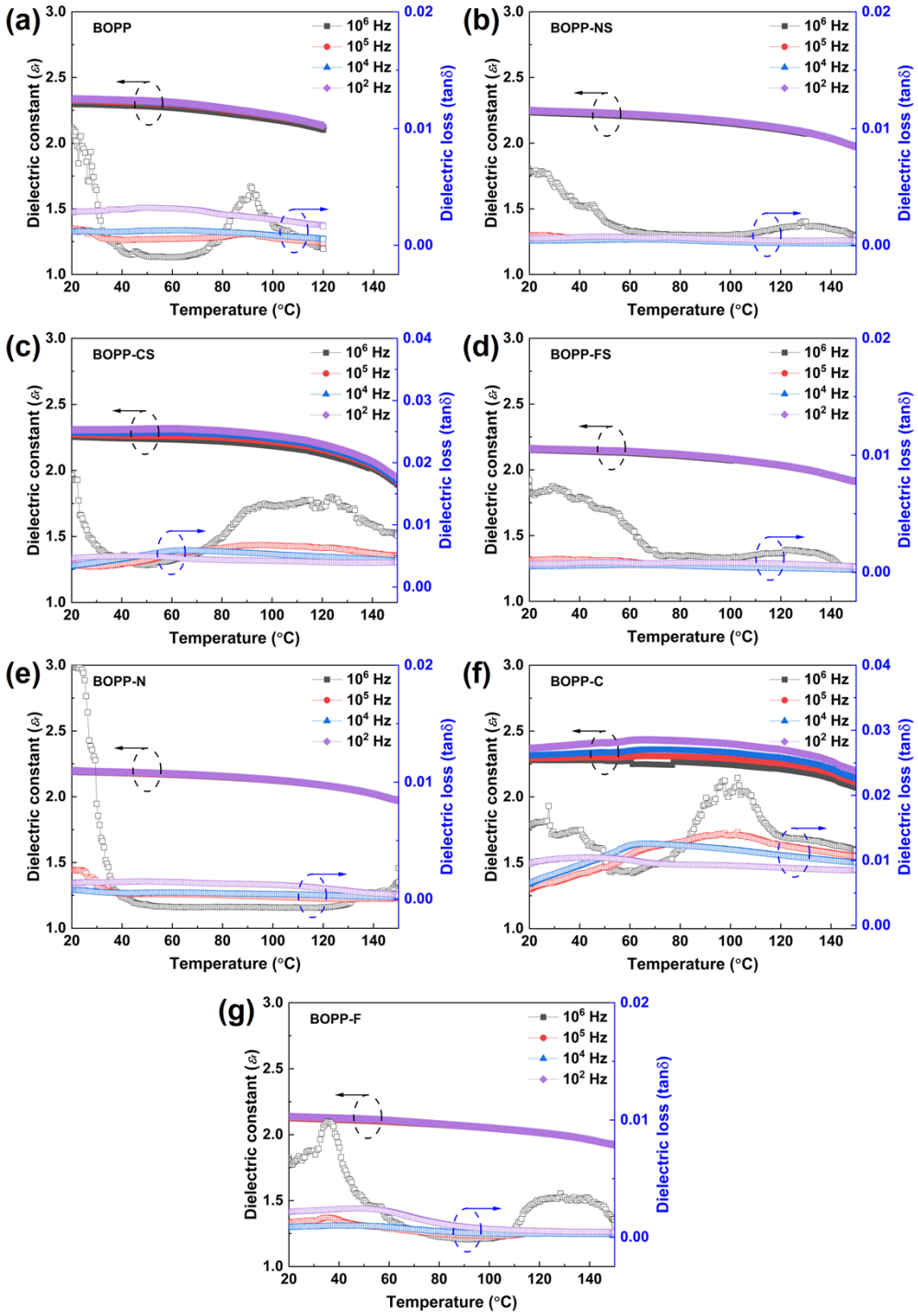

Fig. S7. Dielectric constant (ε_r) and dielectric loss (tanδ) as a function of temperature at different frequencies for BOPP–XS and BOPP–X films.

E_b of polymer films is repeatedly examined in various spots, and the experimental results are evaluated by the two–parameter Weibull analysis, as illustrated by **equation (S3)**,

$$F(x) = 1 - exp[-\left(\frac{x}{\alpha}\right)^{\beta}] \quad \text{(S3)}$$

wherein, x is the measured E_b, α is the characteristic breakdown field, at which at least 63.2% of the samples failed, and β is a shape parameter associated with the dispersion of E_b from different spots. All the samples are repeated over 20 times at each temperature and the possibilities ($F(x)$) as a function of the electric field are compared.

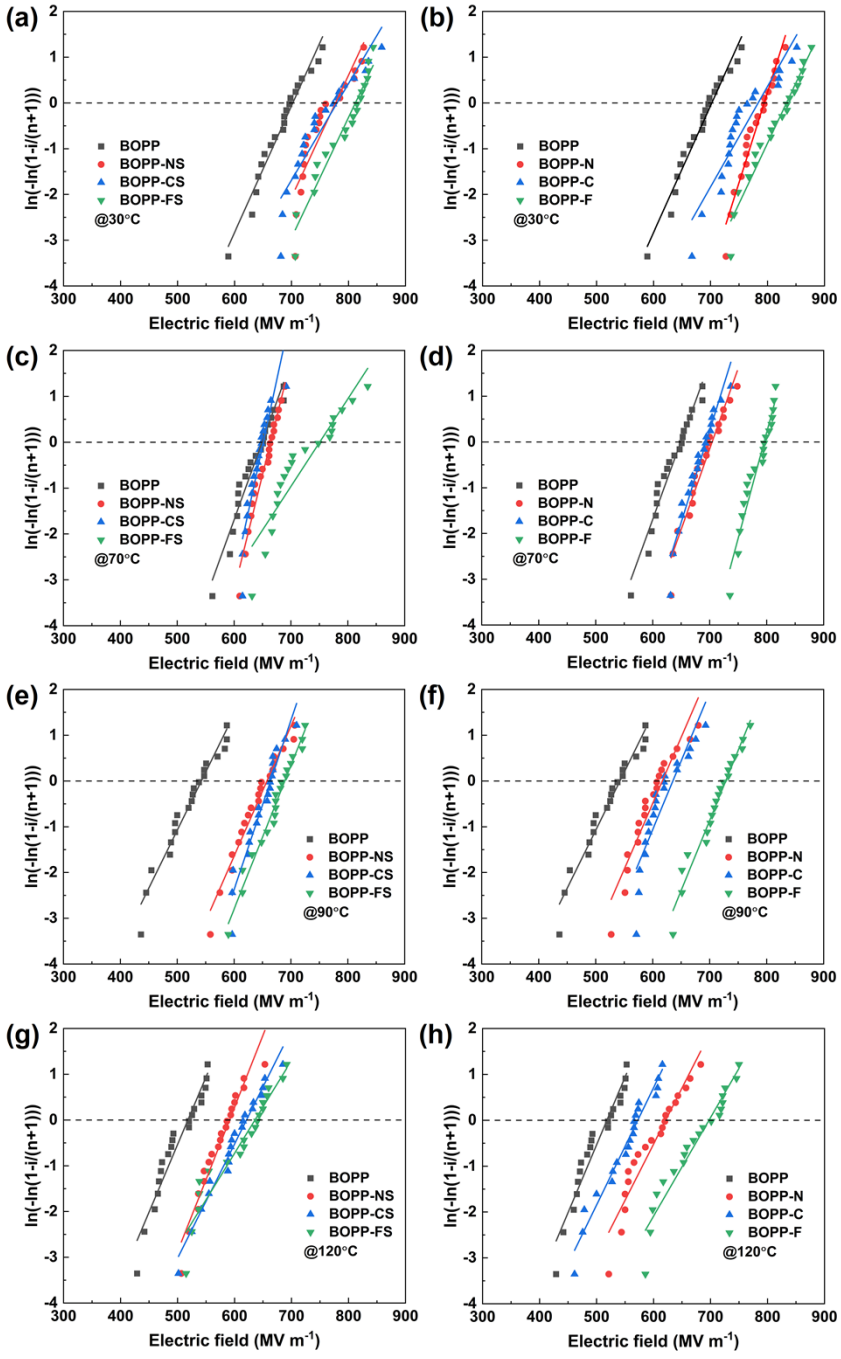

Fig. S8. Weibull distribution of breakdown strength (E_b) of BOPP–XS and BOPP–X films at elevated temperatures.

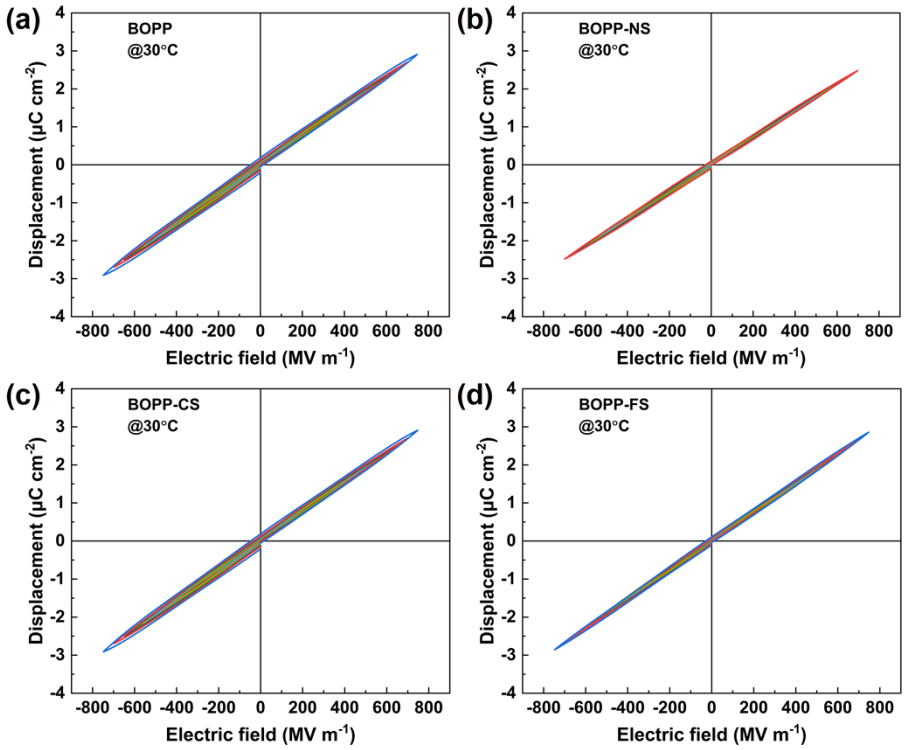

Fig. S9. Bipolar D–E loops of (a) BOPP and (b–d) BOPP–XS films at 30°C.

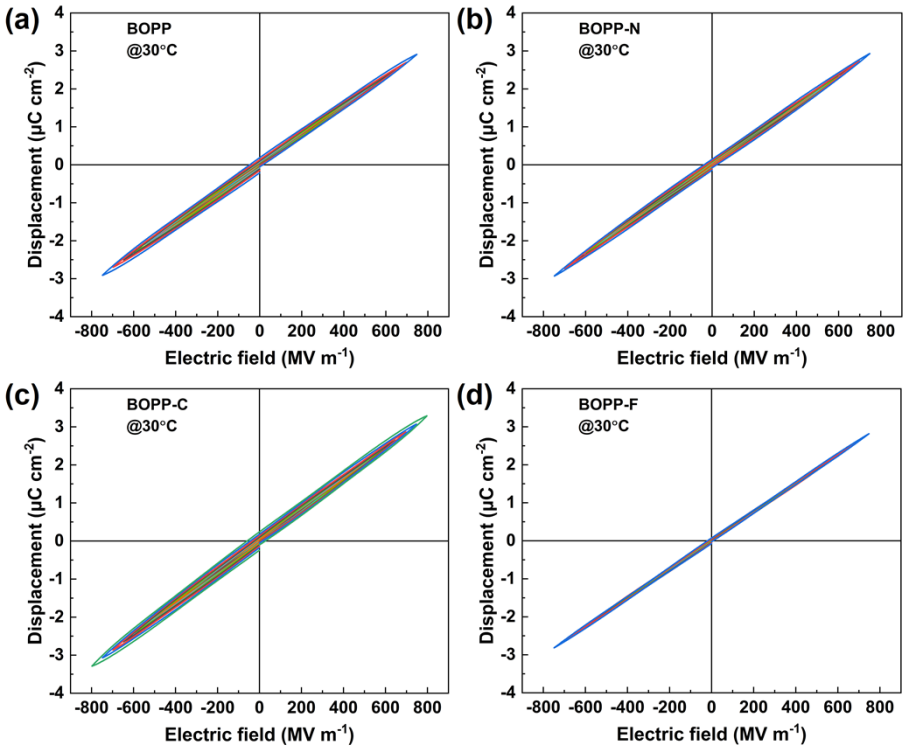

Fig. S10. Bipolar D–E loops of (a) BOPP and (b–d) BOPP–X films at 30°C.

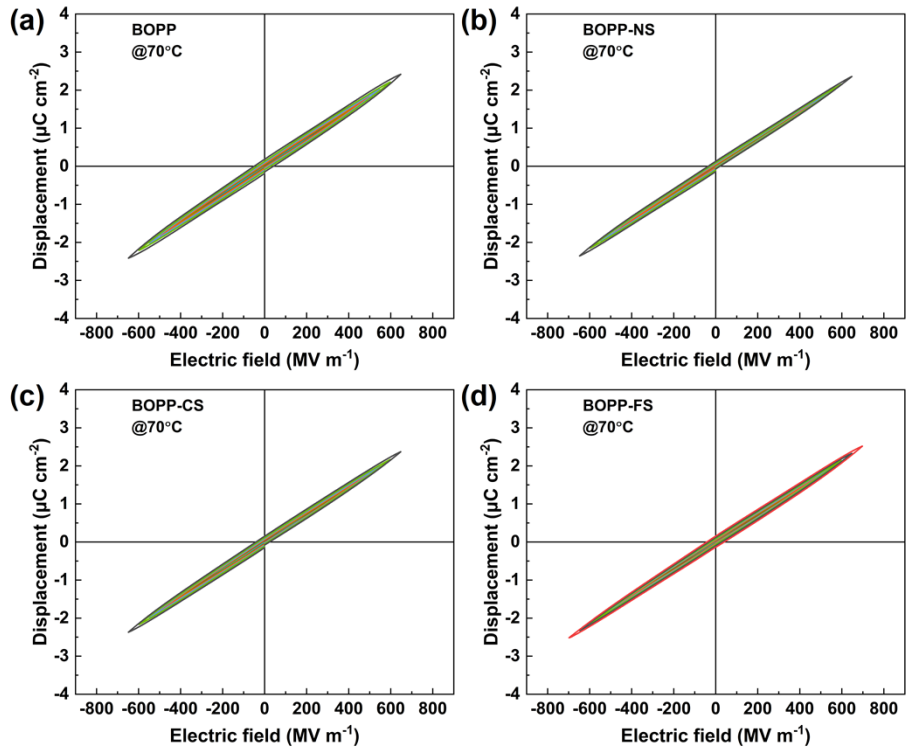

Fig. S11. Bipolar D–E loops of (a) BOPP and (b–d) BOPP–XS films at 70°C.

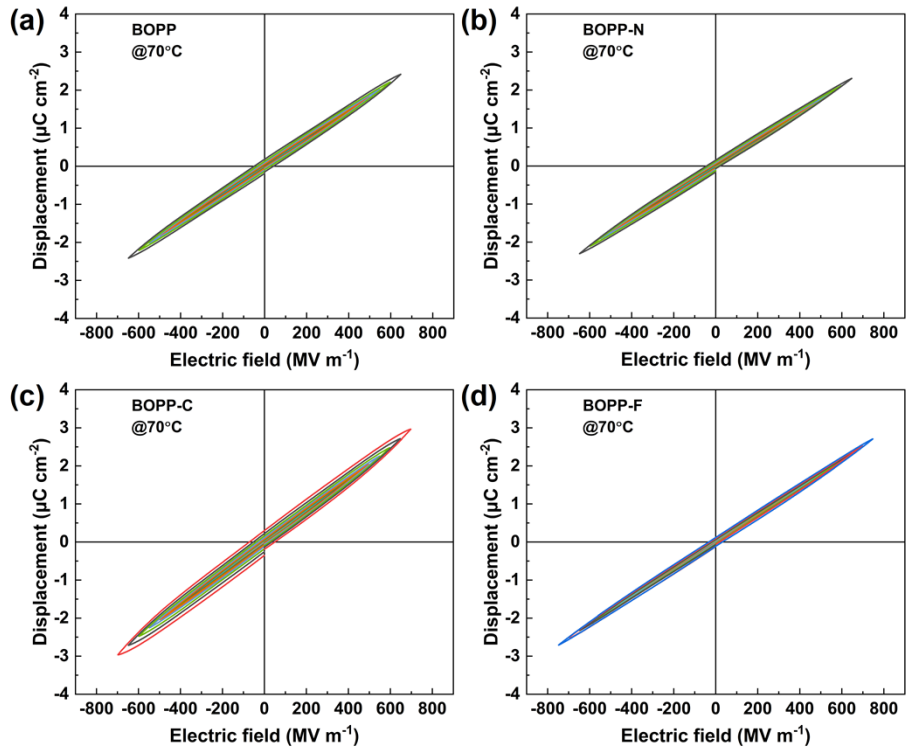

Fig. S12. Bipolar D–E loops of (a) BOPP and (b–d) BOPP–X films at 70°C.

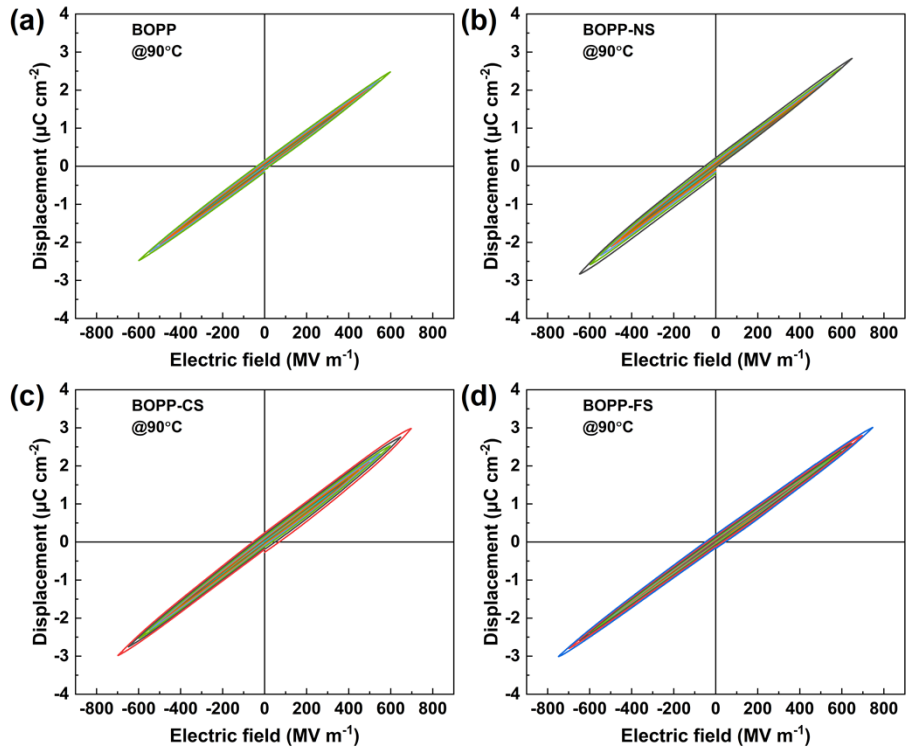

Fig. S13. Bipolar D–E loops of (a) BOPP and (b–d) BOPP–XS films at 90°C.

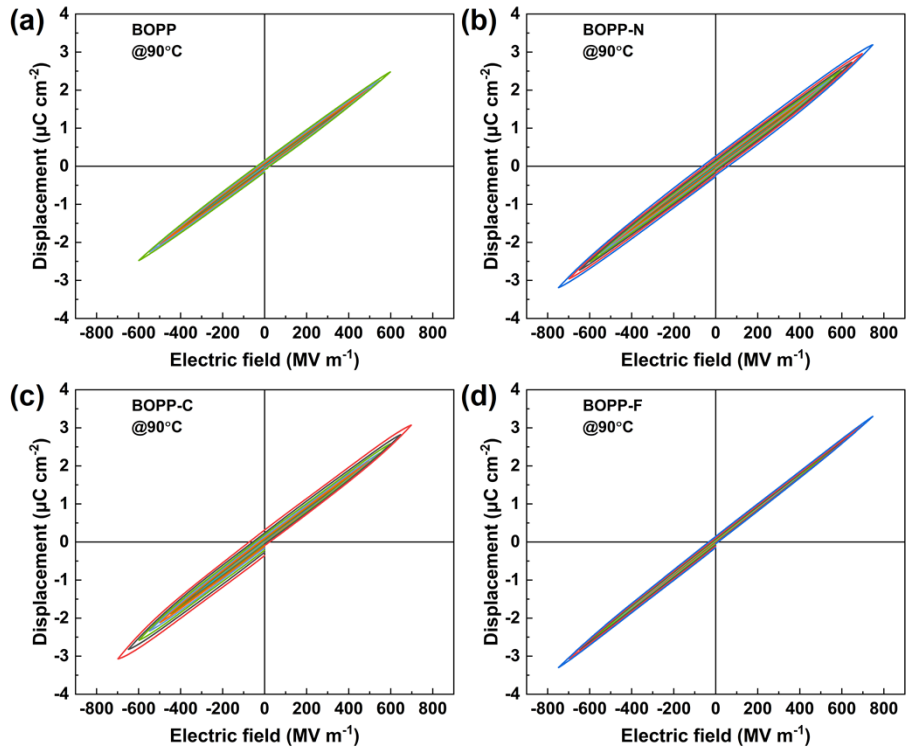

Fig. S14. Bipolar D–E loops of (a) BOPP and (b–d) BOPP–X films at 90°C.

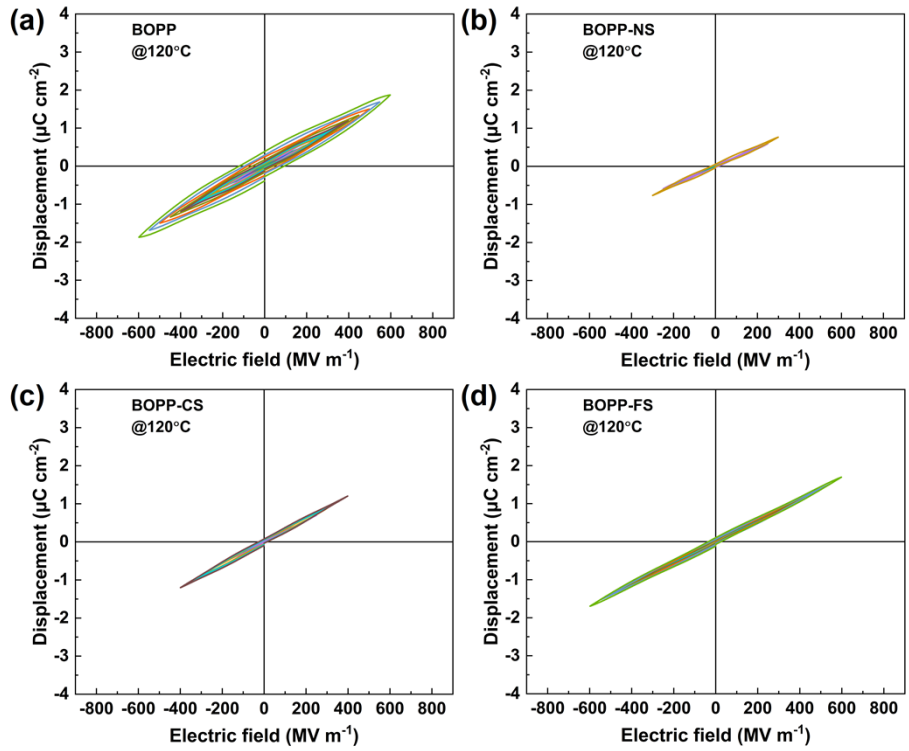

Fig. S15. Bipolar D–E loops of (a) BOPP and (b–d) BOPP–XS films 120°C.

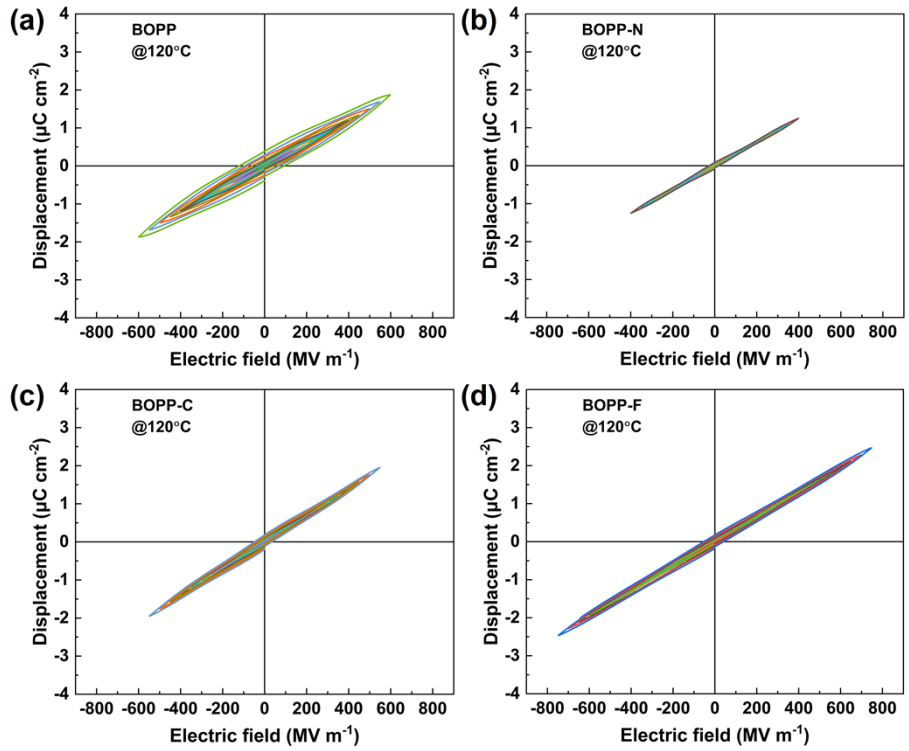

Fig. S16. Bipolar D–E loops of (a) BOPP and (b–d) BOPP–X films at 120°C.

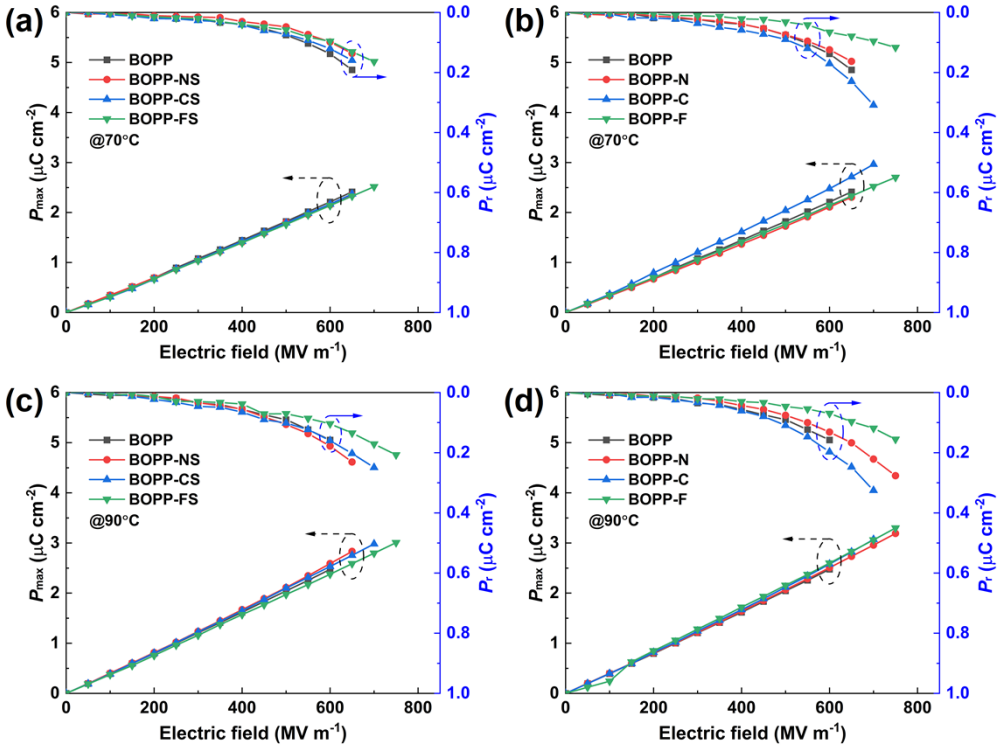

Fig. S17. Displacement of (a,c) BOPP–XS and (b,d) BOPP–X films as a function of electric field at 70°C and 90°C.

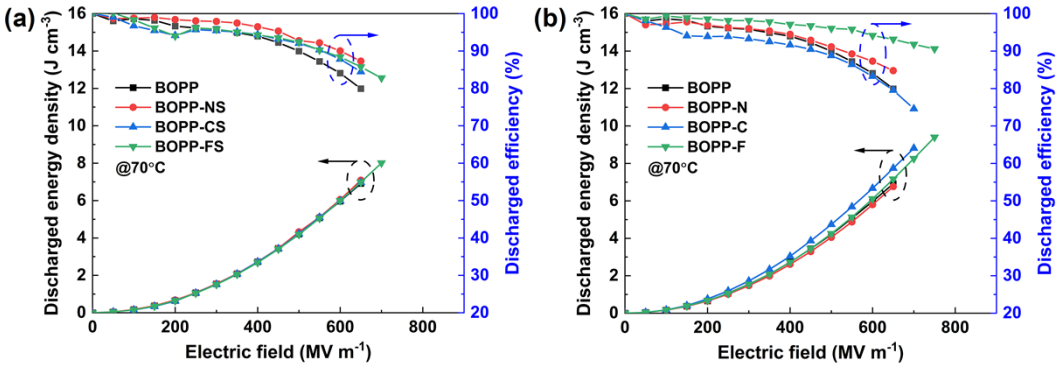

Fig. S18. Discharged energy density and discharged efficiency of (a) BOPP–XS and (b) BOPP–X films at 70°C.

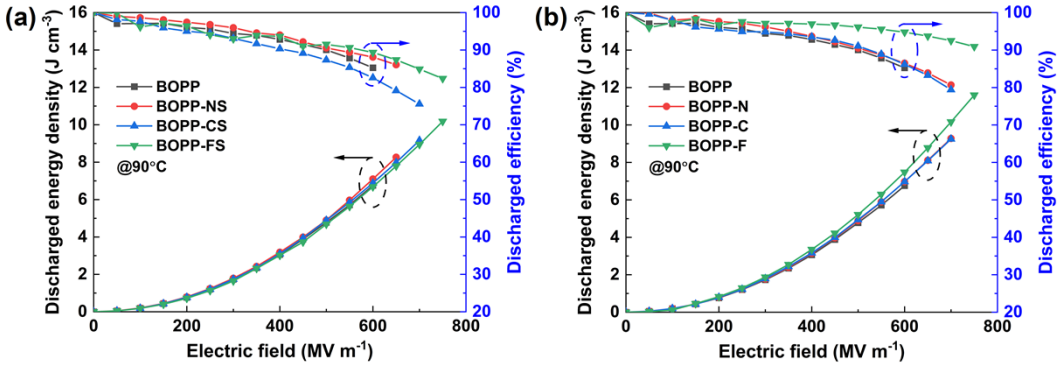

Fig. S19. Discharged energy density and discharged efficiency of (a) BOPP–XS and (b) BOPP–X films at 90°C.

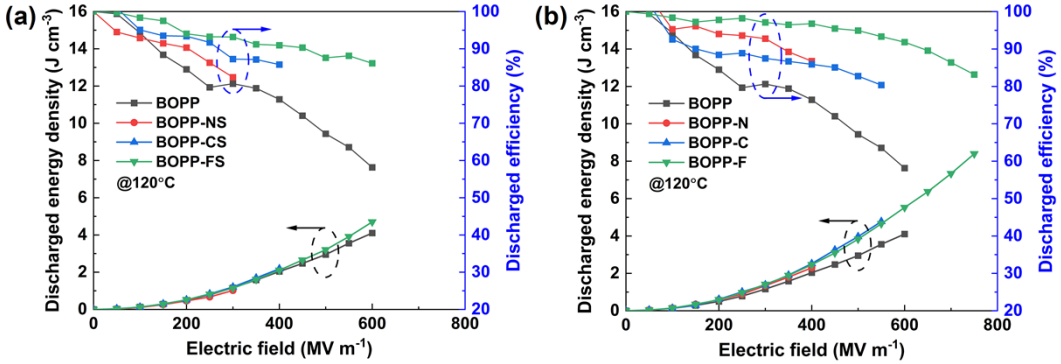

Fig. S20. Discharged energy density and discharged efficiency of (a) BOPP–XS and (b) BOPP–X films at 120°C.

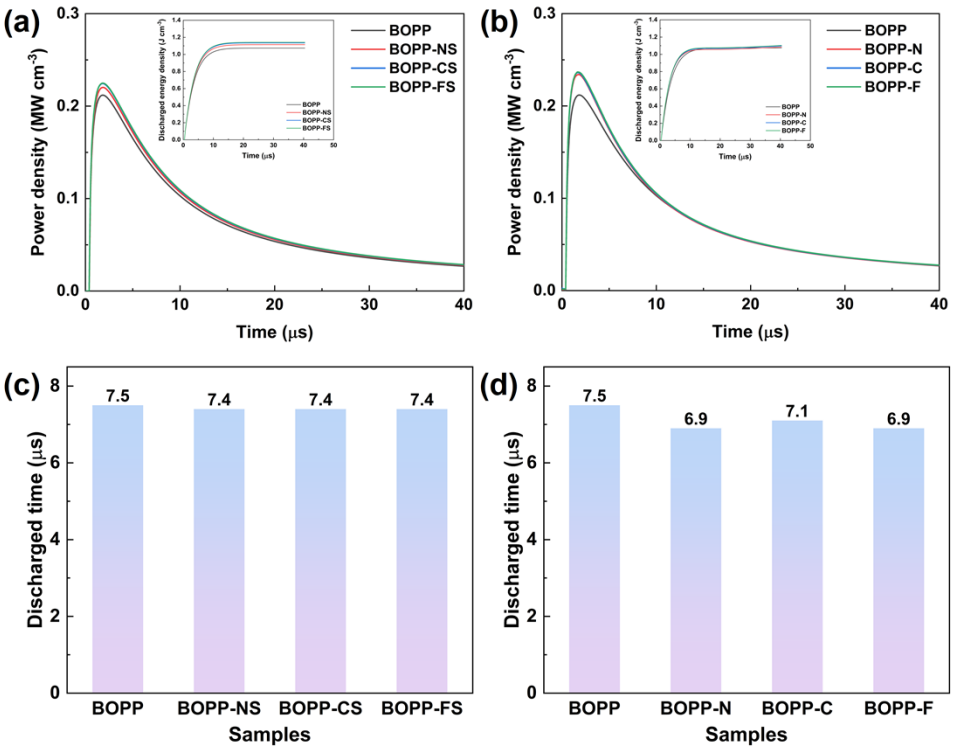

Fig. S21. (a–b) Power density and (c–d) discharged time of BOPP–XS and BOPP–X films. The insets in (a–b) show the discharged energy density calculated from the discharge curve with a discharge–charge instrument under 300 MV m^{-1}, and the inner resistance (R_L) is 100 kΩ.

References

S1. J. Y. Li, F. S. Zhou, D. M. Min, S. T. Li and R. Xia, *IEEE Trans. Dielectr. Electr. Insul.*, 2015, **22**, 1723-1732.

S2. J. G. Su, B. X. Du, T. Han, J. Li, Z. L. Li and M. Xiao, *Compos Part B-Eng*, 2019, **178**.

S3. B. Y. Zhang and G. X. Zhang, *J. Appl. Phys.*, 2017, **121**.